Radiation information for designing and interpreting biological experiments onboard missions beyond low Earth orbit

T. Straume[1], T. Slaba[2], S. Bhattacharya[1], L.A. Braby[3]
[1]NASA Ames Research Center, Moffett Field, CA 94035
[2]NASA Langley Research Center, Hampton, VA 23681
[3]Texas A&M University, College Station, TX 77843

Abstract: There is growing interest in flying biological experiments beyond low-Earth orbit (LEO) to measure biological responses potentially relevant to those expected during a human mission to Mars. Such experiments could be payloads onboard precursor missions, including unmanned private-public partnerships, as well as small low-cost spacecraft (satellites) designed specifically for "biosentinel" type missions. Designing such experiments requires knowledge of the radiation environment and its interactions with both the spacecraft and the experimental payload. Information is provided here that is useful for designing such experiments.

Introduction

Understanding the impact of the space environment on biological systems is becoming particularly important now that extended human missions beyond low Earth orbit (LEO) are being planned (NASA 2016). The radiation environment in interplanetary space, including that expected during future human missions to Mars, is both quantitatively and qualitatively different from that in LEO. The International Space Station (ISS) is a good test platform in LEO to evaluate biological responses to various space-flight factors, including microgravity. However, radiation-induced biological responses evaluated using experiments on the ISS have been difficult to quantify due to low dose rate, relatively few high-LET particles, and the challenges associated with obtaining suitable controls for comparison. This is discussed in a later section "Interplanetary Space *vs* the International Space Station (ISS)".

Biological experiments as secondary payloads associated with unmanned precursor missions are under development to evaluate the space environment beyond LEO and return critical biological response information via telemetry (e.g., Bhattacharya et al. 2016). Such "biosentinel" missions

would be relatively low cost and provide flight opportunities, but are technically and scientifically challenging.

The radiation environment in interplanetary space is complex and consists of galactic cosmic radiation (GCR), which is slowly varying during an 11-year solar cycle, and an occasional (and not yet predictable) solar energetic particle (SEP) event. Radiation flux (and dose rate) from GCR can change by a factor of 2 or more from solar minimum to maximum. The largest dose rate from GCR occurs during solar minimum because the Sun's diminished solar wind permits more charged particles from our galaxy to enter our solar system. Large SEP events, although rare, can be very intense. For an overview of the space radiation environment and its potential risks to astronauts, the reader is referred to Simpson (1983), Townsend (2005), NCRP (2006), Cucinotta et al. (2013), and Straume (2015).

The emphasis here is to provide space-relevant radiation information useful for designing biological experiments in space. To that end, we provide: (a) nuclide-specific dose rates for the GCR spectrum in interplanetary space, (b) particle track traversal rates in selected biological targets, (c) relationships between particle flux and dose, (d) comparisons of radiation environment in interplanetary space with that inside the International Space Station (ISS), (e) implications of particle track microstructure, and (f) probability-dose relationships for solar energetic particle events.

Nuclide-Specific Dose Rates

Listed in Table 1 are nuclide-specific dose rates *vs* shielding thickness for GCR radiation in interplanetary space at 1 astronomical unit (AU). Absorbed dose (D) rates and dose-equivalent (DE) rates were calculated using OLTARIS (Singleterry et al. 2011), a validated web-based radiation analysis tool developed by the NASA Langley Research Center. Included are dose rates for selected shielding scenarios and the resultant average quality factors based on ICRP (2007). These quantities are for the 1977 solar minimum GCR conditions (O'Neill 2010) and are scalable for mission duration based on that environment.

It is observed in Table 1 that some nuclides produce much larger dose rates than others. This is in part because of the well-known "even/odd" effect (Simpson 1983), i.e., even numbered nuclei are more stable and therefore relatively more abundant. The lightest elements (Z = 1-4) are

exceptions. A handful of nuclides in the GCR spectrum contribute most of the dose. With 1 g/cm^2 Al shielding, 63% of the D rate is contributed by H and He alone. In contrast, these elements contribute less than 20% of the DE rate behind the same shielding. Four nuclides in the GCR spectrum (Z = 8, 12, 14, and 26) contribute almost half of the DE. Of particular note is that Z = 26 (Fe) contributes almost a quarter of the total DE from GCR for 1 g/cm^2 Al shielding. The total D rate for the GCR spectrum in interplanetary space (with 1 g/cm^2 Al shielding and based on the 1977 solar minimum) was calculated to be 0.38 mGy per day. The D rate obtained from measurements by MSL-RAD en route to Mars in 2012 was 0.48±0.08 mGy per day (Zeitlin et al. 2013). Given the uncertainties and differences in shielding and solar cycle, these are in reasonable agreement.

It is also observed in Table 1 that the nuclide-specific D and DE contributions are affected by shielding. Most notable, the DE contribution from neutrons (Z=0) becomes significant with thicker shields. Small lightly shielded spacecraft do not result in substantial neutron dose because few neutrons are produced via GCR or SEP primary particle interactions and most of those that are produced escape the spacecraft before they can deposit their energy. This is illustrated in Fig. 1 for GCR and a large SEP event interacting with a spherical shield with radius equal to the listed shield thickness. For GCR, the dose rate without neutron contribution (solid circles) is plotted as a function of Al shielding thickness and compared with the dose rate from neutrons produced in the shield (open circles). For SEP, the total dose from the event without neutron contribution (solid circles) is plotted as a function of Al shielding thickness and compared with the dose from neutrons produced in the shield (open circles).

Effective shielding of small biosentinel spacecraft including their payloads is likely to be only a few g/cm^2 and therefore not expected to experience much neutron dose. However, it should be noted that deep-space vehicles for future human missions and habitats will likely have thick shielding and therefore contributions from neutrons and light ions may dominate the total DE (Norbury and Slaba 2014). Such differences will have to be considered when using results obtained from bio-sentinel missions designed with thin shielding to infer biological responses behind the thicker shields expected for human missions (Curtis and Letaw 1989).

Table 1. Nuclide-specific dose rates *vs* aluminum shielding for GCR radiation in interplanetary space at 1 AU.[a]

Nuclide	D Rate (μGy/day)			DE Rate (μSv/day)			Average Quality Factor[b]		
Z	1 g/cm2	10 g/cm2	30 g/cm2	1 g/cm2	10 g/cm2	30 g/cm2	1 g/cm2	10 g/cm2	30 g/cm2
0	0.10	1.01	3.24	1.96	20.60	66.65	20.22	20.34	20.55
1	162.35	216.25	250.70	239.80	323.21	377.80	1.48	1.49	1.51
2	79.58	82.51	69.47	222.81	269.12	283.95	2.80	3.26	4.09
3	0.56	0.56	0.44	0.86	0.89	0.66	1.53	1.58	1.51
4	0.57	0.61	0.52	0.95	1.13	0.95	1.66	1.85	1.84
5	3.12	2.85	2.02	8.40	7.74	5.08	2.70	2.72	2.51
6	16.37	11.66	5.97	68.76	44.45	19.77	4.20	3.81	3.31
7	5.84	4.55	2.60	31.47	23.04	11.77	5.39	5.07	4.53
8	27.75	17.47	7.35	212.92	119.87	44.44	7.67	6.86	6.05
9	0.65	0.77	0.62	5.41	6.30	4.67	8.35	8.20	7.54
10	6.46	4.16	1.83	71.26	42.27	16.99	11.04	10.16	9.28
11	1.59	1.34	0.80	19.66	15.80	8.81	12.35	11.77	10.96
12	12.13	6.99	2.61	178.54	95.74	33.27	14.72	13.70	12.73
13	2.31	1.57	0.73	36.79	23.89	10.52	15.90	15.21	14.40
14	12.19	6.63	2.26	216.57	112.76	36.59	17.76	17.00	16.19
15	0.50	0.47	0.29	9.26	8.62	5.17	18.50	18.33	17.84
16	2.91	1.75	0.68	59.11	35.06	13.34	20.29	20.03	19.62
17	0.64	0.58	0.33	13.93	12.59	7.10	21.62	21.56	21.36
18	1.43	0.98	0.43	32.63	22.35	9.78	22.80	22.92	22.93
19	1.22	0.84	0.38	28.84	20.18	9.16	23.58	24.00	24.32
20	3.57	1.90	0.64	84.44	46.83	16.21	23.63	24.69	25.44
21	0.80	0.65	0.33	18.87	16.03	8.51	23.73	24.84	25.90
22	3.06	1.60	0.55	67.65	37.79	13.56	22.08	23.58	24.73
23	1.59	1.02	0.42	33.97	23.12	10.01	21.43	22.72	23.76
24	3.50	1.87	0.63	71.72	40.72	14.32	20.52	21.83	22.84
25	2.40	1.50	0.57	47.96	31.75	12.54	19.95	21.11	22.02
26	27.75	11.48	2.57	527.98	233.70	54.58	19.03	20.36	21.26
27	0.15	0.07	0.02	2.71	1.40	0.42	18.53	19.72	20.58
28	1.45	0.61	0.13	26.21	11.70	2.69	18.12	19.22	19.97

[a] Calculations using OLTARIS. [b] Based on ICRP 2007.

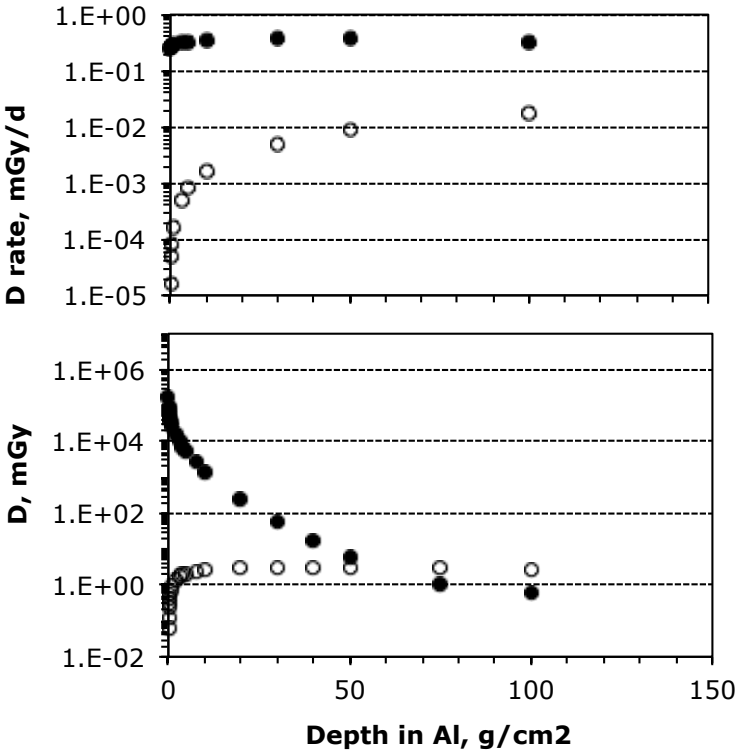

Figure 1. The contribution of neutrons to dose as a function of Al shielding thickness for GCR and SEP radiation. The GCR (top) is dose rate based on 1977 solar minimum conditions and the SEP (bottom) is total dose for the event based on the uncommonly large August 1972 event. Open circles are for neutrons and closed circles are for dose without neutrons. Calculated using OLTARIS with Al sphere shielding.

Particle Track Traversal Rates in Biological Targets

Table 2 provides the calculated integral flux for each nuclide in GCR and the calculated traversals per day for individual cell nuclei (additional considerations are required for multiple cells in a sample, as discussed later). For these examples we assumed a spherical 8 μm diameter mammalian cell nucleus, a 2.5 μm diameter spherical yeast cell nucleus, and an 1 μm x 2 μm rod-like bacterium. The calculations assumed 1977 solar minimum conditions (O'Neil 2010) and 1 g/cm^2 Al shielding. The nuclide-specific flux can be used to estimate traversal rates for any target size, with considerations for shielding, the nature of the biological sample, and solar cycle effects on GCR.

It's important to note that in space, particle traversals are essentially random in both time and direction and for small biological targets such as cells and organelles the traversals are rare (Curtis and Letaw1989). As seen in Table 2, the expected GCR particle traversal rates are substantially less than one per day for any of these biological targets. For a typical mammalian nucleus, the traversal rate is about 1 per week from H plus He but less than 1 per year from the heavy ions. For a yeast nucleus it is about one H plus He traversal every two months, and for a bacterium it is about one per 5 or 6 months.

GCR particles are mostly high energy and will pass through the entire biological sample in a straight line. For a three-dimensional multicellular tissue sample or cells in suspension, this could result in many cells (nuclei) in the sample being traversed by each track. It is also the case that the radiations in space are omni-directional, which could potentially result in two or more tracks passing through the same cell but from different directions. As a result, the data in Table 2, while completely correct, must be used with care. These values represent the averages for individual cells in a tissue sample that is large compared to the distance between individual GCR tracks. However, when one cell nucleus is hit there is a chance that additional cell nuclei along the path of the charged particle will also be hit at essentially the same time. The number of nuclei hit depends on the spacing between nuclei and the characteristics of the cosmic ray particle. This is discussed in more detail under section "Track Structure Considerations".

Table 2. Nuclide-specific flux and mean traversals per day calculated for GCR in inter-planetary space at 1 AU for three hypothetical biological targets.[a]

Nuclide Z	Integral Flux per cm^2-day	Mammalian nucleus[b]	Yeast nucleus[c]	Bacterium[d]
1	3.187E+05	1.60E-01	1.56E-02	6.37E-03
2	3.351E+04	1.68E-02	1.64E-03	6.70E-04
3	1.242E+02	6.24E-05	6.09E-06	2.48E-06
4	7.883E+01	3.96E-05	3.87E-06	1.58E-06
5	2.538E+02	1.27E-04	1.25E-05	5.08E-06
6	8.912E+02	4.48E-04	4.37E-05	1.78E-05
7	2.401E+02	1.21E-04	1.18E-05	4.80E-06
8	8.424E+02	4.23E-04	4.13E-05	1.68E-05
9	1.688E+01	8.48E-06	8.28E-07	3.38E-07
10	1.281E+02	6.44E-05	6.29E-06	2.56E-06
11	2.705E+01	1.36E-05	1.33E-06	5.41E-07
12	1.653E+02	8.30E-05	8.11E-06	3.31E-06
13	2.805E+01	1.41E-05	1.38E-06	5.61E-07
14	1.235E+02	6.21E-05	6.06E-06	2.47E-06
15	4.923E+00	2.47E-06	2.42E-07	9.85E-08
16	2.380E+01	1.20E-05	1.17E-06	4.76E-07
17	4.948E+00	2.49E-06	2.43E-07	9.90E-08
18	9.438E+00	4.74E-06	4.63E-07	1.89E-07
19	7.084E+00	3.56E-06	3.48E-07	1.42E-07
20	1.794E+01	9.01E-06	8.80E-07	3.59E-07
21	3.668E+00	1.84E-06	1.80E-07	7.34E-08
22	1.228E+01	6.17E-06	6.03E-07	2.46E-07
23	5.960E+00	2.99E-06	2.92E-07	1.19E-07
24	1.206E+01	6.06E-06	5.91E-07	2.41E-07
25	7.812E+00	3.92E-06	3.83E-07	1.56E-07
26	8.225E+01	4.13E-05	4.04E-06	1.64E-06
27	4.101E-01	2.06E-07	2.01E-08	8.20E-09
28	3.860E+00	1.94E-06	1.89E-07	7.72E-08

[a] For 1 g/cm^2 Al shielding. Calculations using OLTARIS are based on 1977 solar minimum environment (O'Neil 2010). For single cells only. Sample-dependent adjustments to these calculations are required for multicellular samples.
[b] 8 μm diameter.
[c] 2.5 μm diameter.
[d] 1 x 2 μm rod like bacterium.

The Relationship Between Nuclide-Specific Flux, D, and DE

It is observed in Fig. 2a that the GCR particle flux is strongly weighted toward the lighter elements, primarily H and He. At the high velocities characteristic of GCR these particles have stopping powers in the same range as the secondary electrons produced by x

and γ rays. These low LET values persist until the ions slow to a small fraction of their original velocity. This results in most of the hits in a biological sample being from low Z (and relatively low LET) nuclides.

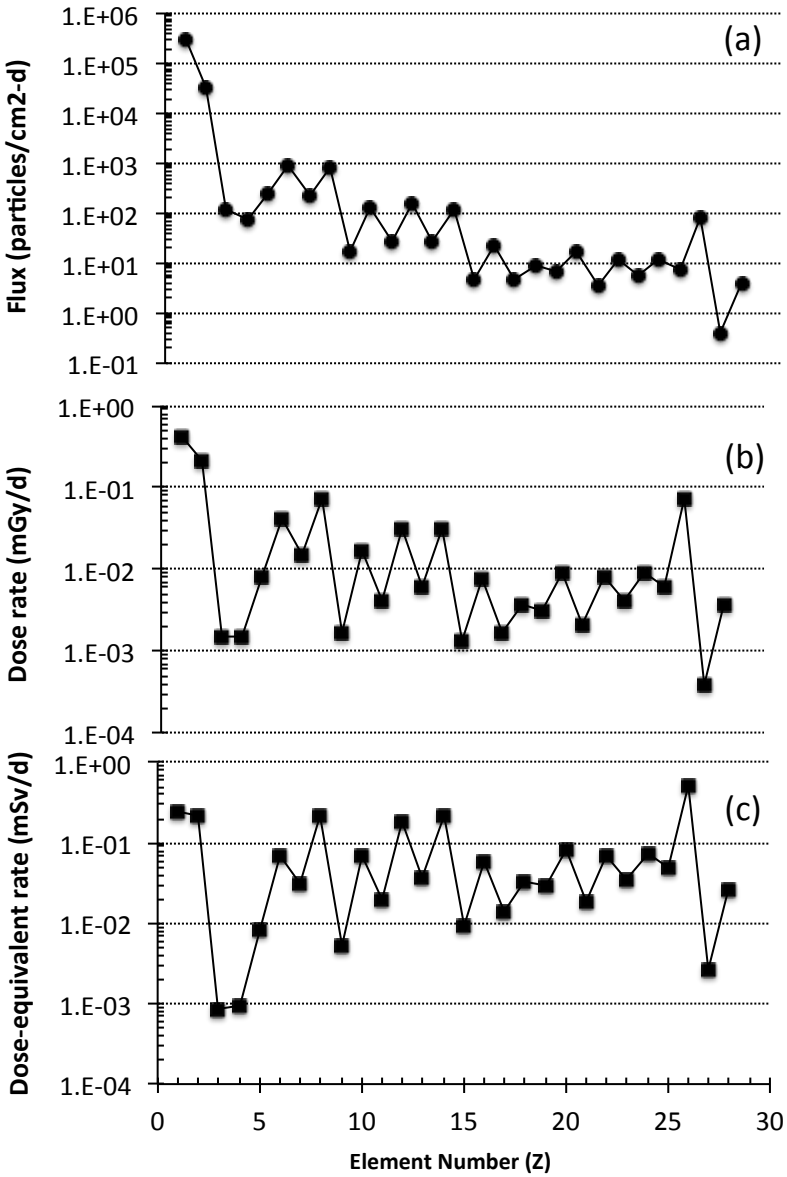

Figure 2. (a) Nuclide-specific flux for GCR spectrum. (b) Nuclide-specific absorbed dose (D) rates for GCR spectrum. (c) Nuclide-specific dose-equivalent (DE) rates for GCR spectrum. All were calculated using OLTARIS for 1977 solar minimum conditions and behind 1 g/cm^2 Al shielding.

In contrast to the flux in Fig. 2a, it is seen in Figs. 2b and 2c that the higher Z elements in GCR contribute relatively more to the D and DE than the lighter elements for thin shielding. This is particularly the case for DE (Fig. 2c). In that case, the highest DE rate is not from H and He but rather from Z=26 (Fe). Also, the time in the solar cycle further modifies the relative contribution of heavy ions to the fluence and dose. At solar maximum the dose is reduced due to the lighter ions being deflected by the solar wind. Due to their greater magnetic rigidity the fluence of heavy ions is reduced very little, and therefore they become an even more dominant part of the radiation spectrum. Hence, both shielding and solar cycle can have important implications for biological experiments in deep space, especially for biological endpoints with large relative biological effectiveness (RBE), which can be identified using ground-based simulated space radiations.

The above is for thin shielding (1 g/cm^2 Al). As shielding is increased (Fig. 3), the heavier elements are impacted relatively more than the lighter elements. For example, Z=26 (^{56}Fe) produces a larger DE than either H or He with a 1 g/cm^2 shield, but much smaller DE when shielding thickness is increased to 30 g/cm^2. This effect is mainly due to nuclear interactions resulting in fragmentation of the high Z nuclides into a spectrum of lighter particles and nucleons. In fact, one can see from Fig. 3 that as shielding is increased, the DE for H and He actually increases, reflecting gains in their flux from the break-up of heavier ions. Again, this can be an important consideration depending on spacecraft design and placement of the bio-experiment within the spacecraft.

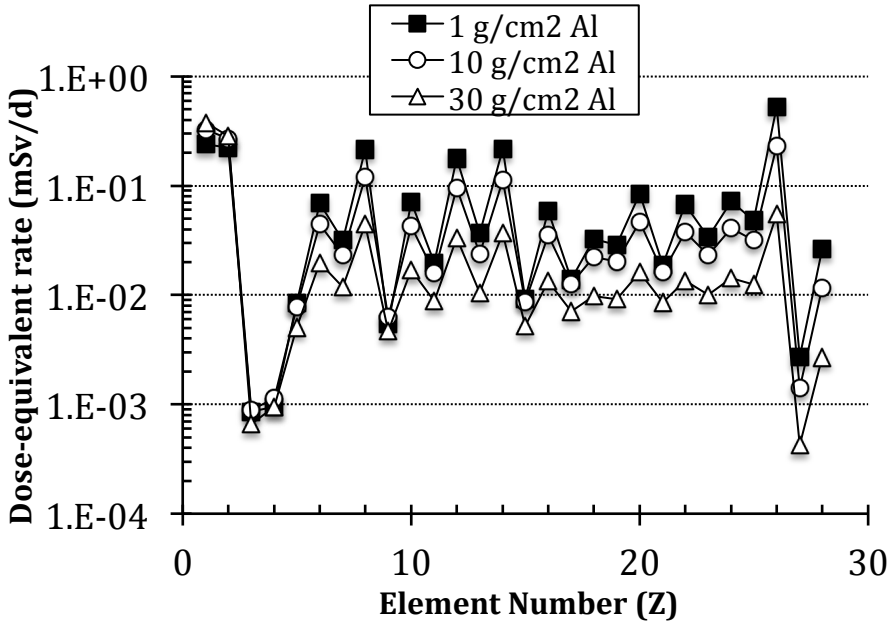

Figure 3. Influence of shielding on nuclide-specific dose-equivalent (DE) rates for GCR spectrum. Calculated using OLTARIS for solar minimum conditions.

Interplanetary Space vs the International Space Station (ISS)

A major purpose for the ISS is to use it as a space research platform. It is therefore instructive to compare the radiation environment inside the ISS with that in interplanetary space at 1AU. Dosimetric quantities are compared in Table 3. Two observations are most notable: (1) the dose rate is substantially higher in interplanetary space than inside the ISS even for comparable shielding, and (2) the quality factor (Q) is substantially larger in space with light shielding than inside the ISS. These two differences converge to make it more likely that radiation-induced biological responses may be detected on a lightly shielded biosentinel mission in interplanetary space than on the ISS. Biological experiments onboard the ISS would only receive about 0.08 Gy during a 12-month mission. This is below or approaching the lower limit of detection for most biological endpoints and would be challenging for providing statistically significant data when comparing with "unexposed" controls. Beyond LEO, the combination of higher dose rate and larger Q (i.e., relatively more high LET particles) increases the chances that biological effects may be detected. Importantly, this is a key rationale for biosentinel-type missions.

Table 3. Comparison of dosimetric quantities inside the ISS and in interplanetary space with various thicknesses of Al shielding.

Location	D (mGy/d)	DE (mSv/d)	Q
ISS (service module)	0.22	0.50	2.3
Space (1g/cm^2)	0.38	2.34	6.1
Space (10g/cm^2)	0.38	1.65	4.3
Space (30g/cm^2)	0.36	1.10	3.1

These results are further illustrated in Fig. 4 where nuclide-specific flux inside the ISS is compared with that in interplanetary space for various thicknesses of Al shielding. The median shielding inside the ISS service module is about 20 g/cm^2 Al and the shield thickness for a deep space human mission will likely range from 20 g/cm^2 to 40 g/cm^2.

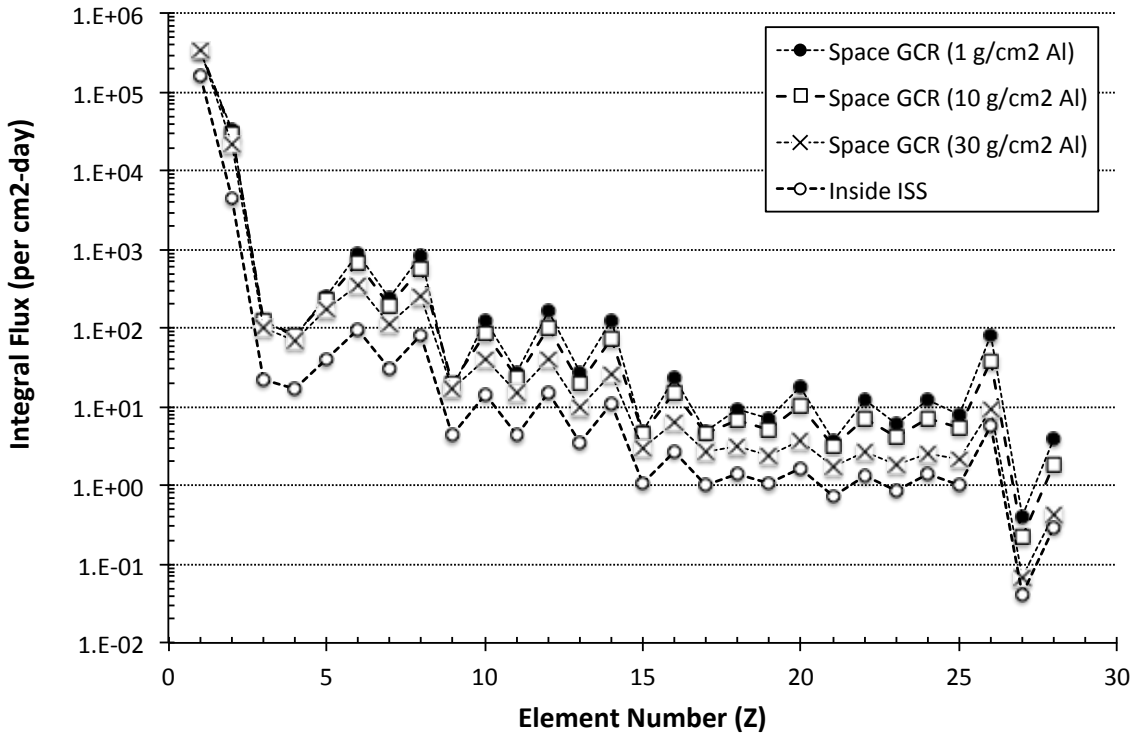

Figure 4. Comparison of nuclide-specific flux inside the ISS service module with that calculated for interplanetary space at 1 AU with 1, 10, and 30 g/cm^2 Al shielding. Based on modeling calculations using OLTARIS and 1977 solar minimum environment (O'Neil 2010).

It is noted in Fig. 4 that as shielding is increased in interplanetary space to thicknesses comparable to the ISS the differences between the nuclide-specific particle flux inside a deep space vehicle and inside the ISS are reduced, but not eliminated. This difference can be attributed to the geomagnetic field and terrestrial blockage, which attenuate ISS exposures compared to free space. Behind only 1 g/cm^2 of Al shielding, integral flux values for heavy ions ($Z > 2$) were noticeably larger, as would be expected, and suggests that biosentinel missions will encounter a radiation environment with a larger concentration of high LET particles compared to what astronauts might encounter in deep space or in the ISS. This must be taken into account when using information obtained from lightly shielded experiments to estimate risk associated with heavier shielded deep-space human missions.

Track Structure Considerations

The number of track traversals and energy deposited per traversal are not the only considerations for radiation damage in the biological sample. The ionizing particle track itself must be considered. The track can be thought of as composed of a core of dense ionizations and a penumbra of delta rays (electrons) emitted radially from the core. The core of a high Z particle track produces very dense damage (high LET) and for heavy ions is often lethal to the cell if traversing the nucleus. The penumbra is less dense (consisting of lower LET electron tracks) and produces a dose distribution that decreases with the square of the distance from the core center (Chatterjee and Schaefer 1976, Chatterjee and Holley 1993). There is no sharp distinction between the core and penumbra or cutoff at the limit of the penumbra. The values given by the Chatterjee model are intended to represent regions relevant to radiation chemistry processes.

An illustration of the sizes of the track core and penumbra as a function of particle kinetic energy is provided in Fig. 5. It is seen that the core radius is small compared to dimensions of biological cells and organelles and will therefore require a rather precise hit to damage a target via direct action. The radius of the core is less than about 0.01 μm for essentially all GCR and solar particle radiations. In contrast, the penumbra (delta rays) emanating from the core is much larger and can extend to more than 1 mm for very

high-energy particles, and therefore can deposit energy in biological targets at substantial distances away from the central particle track.

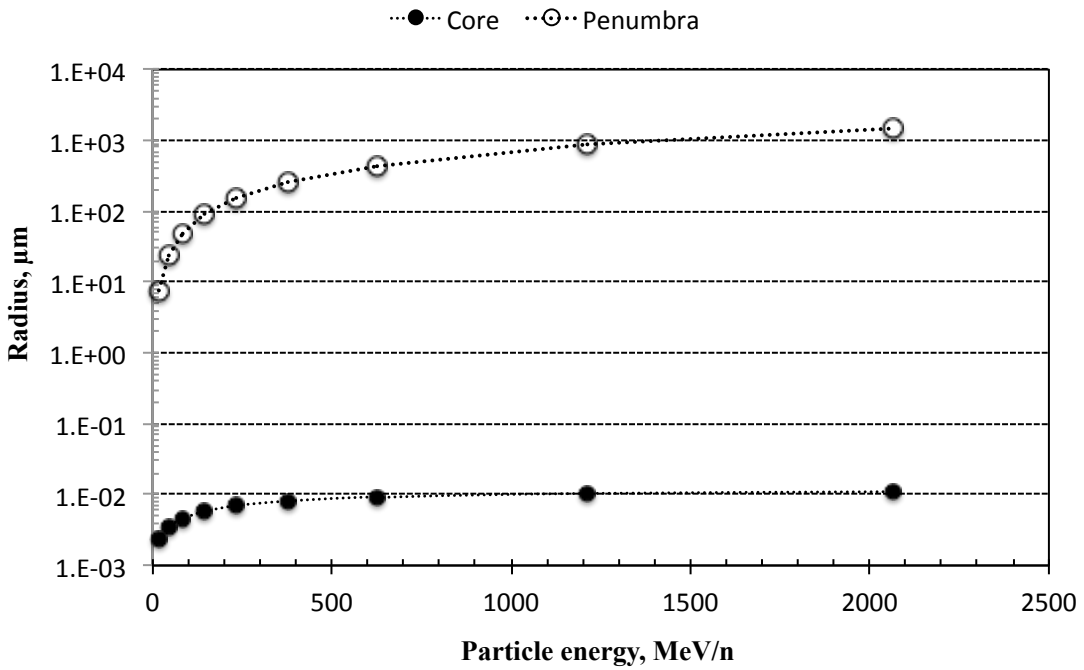

Figure 5. Core radius and penumbra (delta-ray) radius as a function of particle energy. Plotted from data provided in Chatterjee and Schaefer 1976, which are empirically derived based on particle tracks in an aqueous medium.

A subsequent derivation of the radius of the core and penumbra was presented in Chatterjee and Holley (1993), and provides similar results, albeit some differences are apparent in the penumbra radius at the highest particle energies. However, as previously mentioned, there is no sharp cutoff at the limit of the penumbra and the differences in the derivations do not have practical implications for this paper.

Dose in the track core (D_c) as well as from delta rays (D_p) at various distances from the track center can be calculated for single particle tracks using Eqns. 1 and 2 below obtained from Metting et al. 1988.

$$D_c = 16\ (L/2)/\pi\ r_c^2 + (L/2)/2\pi\ r_c^2\ \ln(2.718*r_p/r_c). \qquad \text{Eqn. 1}$$

$$D_p = 16\ (L/2)/(2\pi\ b^2\ \ln(2.718*r_p/r_c). \qquad \text{Eqn. 2}$$

where D is in cGy, L is the unrestricted LET in keV/µm, r_c and r_p are the radius of the core and penumbra in µm, and b is the radial distance from the center of the core in µm.

In the above equations, inserting r_c and r_p calculated by the method provided in Chatterjee and Schaefer (1976) for 250 MeV protons, 200 MeV/n ^{12}C, and 1 GeV/n ^{56}Fe, and the corresponding L for these particles, provides the results in Fig. 6. It is observed that the mean (expected) dose in the track core is high for all particles and that the dose from delta-rays diminishes sharply with distance from the core. From these results one may infer that to receive a dose from delta-rays large enough to provide a detectable response in a biological system would require the "target" to be in close proximity to the track core. For example, the expected delta-ray dose from a 1 GeV/n ^{56}Fe particle is about 16 cGy at 1 µm and only about 1 cGy at 4 µm, which would require a very sensitive biological endpoint to detect. It has been suggested that beyond 4 µm the targets would be hit by only single electron events, which are unlikely to result in a detectable biological response (Curtis 2012).

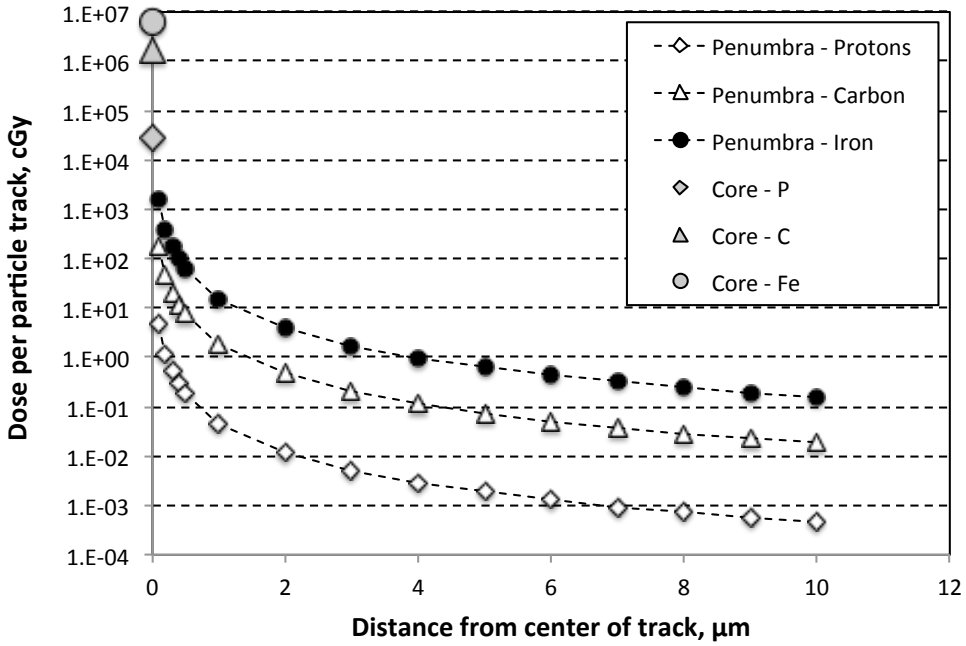

Figure 6. Estimates of average dose (expected value) in single particle tracks from 250 MeV protons, 200 MeV/n ^{12}C, and 1 GeV/n ^{56}Fe. Doses are provided for the track core itself and for the penumbra at various distances from the core.

It should be noted that both the track core and the penumbra have fine structure (Chatterjee and Holley 1993), which can impact the biological response. The core contains "spurs" that depend on Z and velocity. For light ions such as H and He, the spurs are widely spaced along the length of the core, and for heavy ions, the spurs overlap forming a continuous column. In the penumbra, the delta-ray electrons are separated from each other by relatively large distances along the primary track, which results in a small average dose from delta rays because a large fraction of the cells have no energy deposition. However, if a small sensitive target (e.g., DNA) is hit by a delta-ray electron it can deposit much more energy than inferred from the average absorbed dose (Braby 2008). Evaluating such fine structure would require Monte Carlo modeling, which is beyond the scope of this paper.

Biological samples employed in biosentinel experiments can be of various forms, e.g., cells in dry state, cells in suspension, cells in a monolayer adhering to a surface, or multicellular tissue (which could be either a sample or an entire organism). The form of the sample can influence the microdosimetry and therefore the biological response to the radiation environment. Cells that can exist for extended periods of time in the dry state and then begin growing only after a liquid medium is added could be particularly useful for extended biosentinel-type missions in deep space. An example of such biological systems would be yeast, which will be employed in an upcoming NASA BioSentinel mission using sensitive genetically-engineered strains (Bhattacharya et al. 2016).

For a sparse monolayer of cells on a flat surface, the likelihood of a track passing through two or more cells is very small. Under such conditions, it is observed in Fig. 7 that only the two lightest elements (Z = 1-2) are expected to traverse every yeast cell nucleus during missions lasting 3 to 18 months. The expected average hits per nucleus from these elements range from about 1.5 at 3 months to almost 10 at 18 months. The heavier elements are very unlikely to produce multiple traversals in a nucleus during the mission. This makes it particularly important to consider sample size (the number of cells per sample) when designing the experiment, i.e., the expected number of cells traversed per sample would be the probability of traversals per cell times the number of cells per sample.

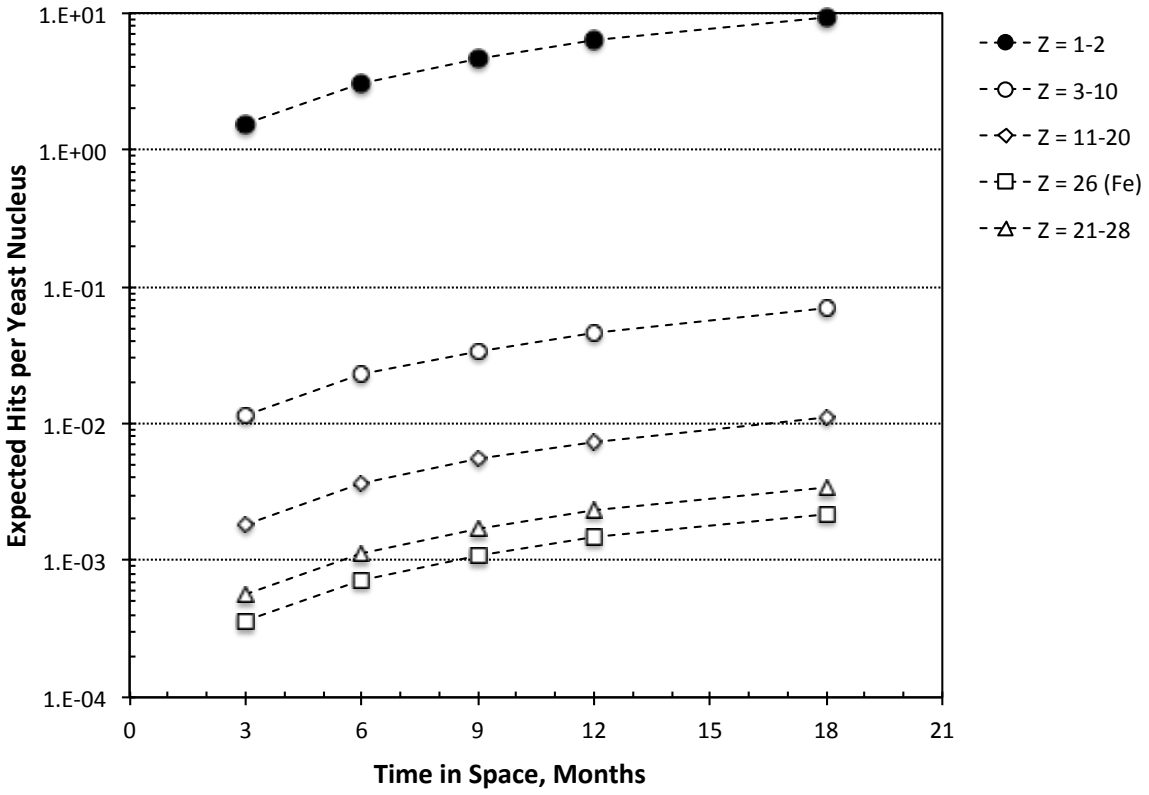

Figure 7. Particle track traversals per yeast nucleus if single layer on a flat surface as a function of time in interplanetary space. For selected groupings of Z as indicated in the Figure legend.

Fig. 8 shows the Poisson distribution (Haight 1967) of Z = 1-2 traversals through a yeast nucleus during 12 months in interplanetary space. The expected value is 6.3 traversals per nucleus. The probability of no traversals is small, 0.2%. This implies that 99.8% of the nuclei will be traversed by at least one H or He particle during 12 months in space. If the traversals are randomly distributed over time, an average of about one traversal every 2 months would be expected. This is a long time between hits such that one would expect the GCR environment to produce effects characteristic of low dose-rate exposures.

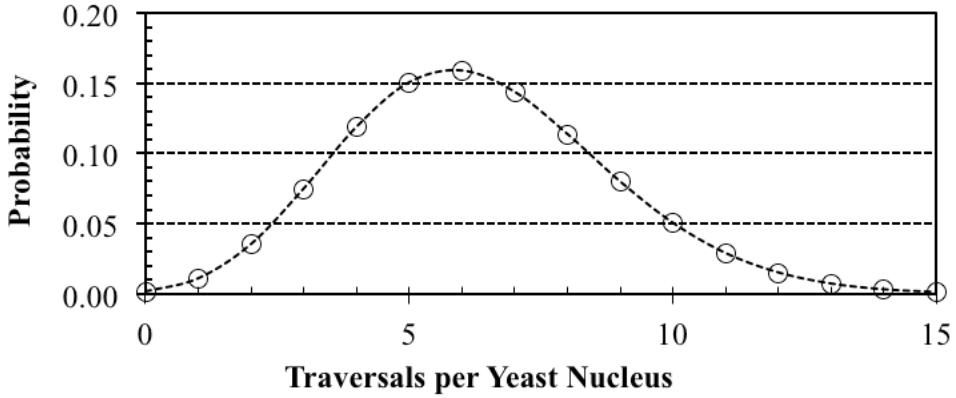

Figure 8. The Poisson distribution of GCR traversals (Z = 1-2) per yeast nucleus during 12 months in interplanetary space.

Traversal probabilities were also calculated for the other GCR nuclides during 12 months in space.

P (Z=3-10) = expected value is 0.0461, at least one hit is 0.045, no hits is 0.955.

P (Z=11-20) = expected value is 0.0074, at least one hit is 0.007, no hits is 0.993.

P (Z=21-28) = expected value is 0.0023, at least one hit is 0.002, no hits is 0.998.

P (Z=26) = expected value is 0.0015, at least one hit 0.001, no hits is 0.999.

Assuming 10^5 cells are uniformly distributed in a monolayer on the bottom of a 5 mm diameter well, approximately 160 will be within the penumbra of a 200 MeV/n particle, as described by Chatterjee and Schaefer (1976). Using Eqn. 2, the dose at a given distance from the core can be estimated for tracks perpendicular to the cell monolayer. In this case, the "dose" is the average energy per mass for cells hit by delta rays and cells not hit. The energy per mass for single delta ray events is approximately 0.9 cGy (Metting et al 1988) so if, for example, the average dose at a particular distance from the center of the track is 0.1 cGy approximately 11% of the yeast nuclei at that distance would be hit by a delta ray, i.e., (0.1/0.9) x 100. In the dry state there will be only gas or vacuum on the top side of the monolayer, particles approaching from the top will not produce delta ray equilibrium at the monolayer and will produce somewhat less energy imparted per mass resulting in a smaller fraction of cells hit by delta rays.

For cells in suspension, if 10^5 cells are dispersed in 100 μL solution, the cell concentration based on cell volume-to-solution volume would be about 1.1 x 10^{-4}. Although this would be a dilute cell suspension with substantial average distance between cells, a track (core plus penumbra) passing through the cell suspension would have a significant probability of passing through more than one cell nucleus. Assuming random positioning of the cells in the well, each cell would occupy a neighborhood measuring 100 x100 x 100 μm, then each track would on average traverse about 46 of these neighborhoods, i.e., $(10^5)^{0.33}$. Because of the very small cross-sectional area of the track core there is only a 0.022 probability that a nucleus (yeast used for this example) will actually be hit by a single-track core passing through the suspension of cells described above. For the flux and spectrum of GCR particles in interplanetary space the expected number of track core traversals of nuclei in a sample of 100,000 yeast cells during a 12-month mission would be 6.31×10^5 (Z = 1-2), 4.61×10^3 (Z = 3-10), 7.38×10^2 (Z = 11-20), and 2.30×10^2 (Z = 21-28).

In contrast, the penumbra is much larger than the core and therefore has much greater probability of hitting the nucleus. Listed in Table 4 are the calculated average doses and number of delta-ray hits per nucleus at selected distances from the core center of individual tracks for 1 GeV/n ^{56}Fe, 200 MeV/n ^{12}C, and 250 MeV protons. Again, these are delta-ray hits from a single track passing through the cell suspension described above. For a yeast nucleus, one delta ray hit is estimated to result at about 4 μm from a 1 GeV/n ^{56}Fe track, at about 1.5 μm from 200 MeV/n ^{12}C, and at <0.3 μm from a 250 MeV proton track. At larger distances the probability of a nucleus being hit by a delta ray decreases rapidly. For most biological endpoints a single delta-ray hit (0.9 cGy for a yeast nucleus) may be neglected (Curtis 2013), but for some very radiosensitive endpoints it could potentially be significant.

The number of delta rays per nucleus during a mission in interplanetary space would be proportional to the integral particle fluence in the biological sample. Detailed Monte Carlo track simulation calculations are needed to produce accurate probabilities for delta ray interactions in cell nuclei at specific distances from GCR tracks. The results in Table 4 are estimates derived from the absorbed dose as a function of distance and measured characteristics of HZE tracks (Brooks et al. 2001, Metting et al. 1988).

Table 4. Expected doses and nuclear hits from delta rays as a function of distance from the center of a particle track.[a]

Distance (µm)	1-GeV/n ^{26}Fe		200 MeV/n ^{12}C		250-MeV ^{1}H	
	D (cGy)	Number of delta rays per nucleus	D (cGy)	Number of delta rays per nucleus	D (cGy)	Number of delta rays per nucleus
0.1	1570	1744	187	208	4.65	5.16
0.3	174	194	21	23	0.52	0.57
0.4	98	109	12	13	0.29	0.32
0.5	63	70	7.5	8.3	0.19	0.21
1	16	17	1.9	2.1	0.046	0.052
2	3.9	4.4	0.47	0.52	0.012	0.013
3	1.7	1.9	0.21	0.23	0.0052	0.0057
4	0.98	1.09	0.12	0.13	0.0029	0.0032
5	0.63	0.70	0.075	0.083	0.00186	0.0021
10	0.16	0.17	0.019	0.021	0.00047	0.00052
25	0.025	0.028	0.0030	0.0033	0.0000743	0.000082
50	0.0063	0.0070	0.00075	0.00083	0.0000186	0.000021
100	0.0016	0.0017	0.00019	0.00021	0.0000046	0.000005

[a] From a single particle track traversing the center of a yeast nucleus.

Solar Particle Events and Solar Cycle Considerations

The Sun's activity cycles from low to high with about an 11-y period, which has been observed to vary from 9 y to more than 12 y. The variation in the Sun's activity includes changes in the levels of solar radiation and ejection of solar material and changes in the number of sunspots, flares, and other manifestations. Even with their periodicity, it is not possible at present to accurately predict future minima and maxima. Hathaway (2016) has recently extrapolated the current solar cycle (Cycle 24) to 2020. Given the uncertainties, his estimate suggests the next solar minimum will occur in the 2019 - 2021 time period, which may be an important consideration for biosentinel-type experiments in the planning phase.

Due to their stochastic nature, SEP events are generally modeled probabilistically (Xapsos et al. 1999). Fig. 9 illustrates such estimates of the dose expected from SEP events

in interplanetary space at 1 AU during solar maximum conditions. The results are for 18 mo duration and two shielding thicknesses, 0.3 g/cm^2 (1.1 mm) and 1 g/cm^2 (3.7 mm) Al.

Based on these modeling calculations, there is a 50% chance that a dose of 48 cGy or greater will be received from SEP events during an 18-mo mission in deep space with 0.3 g/cm^2 (1.1 mm) Al shielding. This is reduced to 15 cGy with 1 g/cm^2 (3.7 mm) Al. There is a 10% chance for a dose of at least 356 cGy and 161 cGy behind 0.3 g/cm^2 and 1 g/cm^2, respectively. As can be seen in Fig. 9 even larger doses are possible, but unlikely. SEP events are less likely to occur during solar minimum compared to solar maximum. However, for biosentinel type missions with thin shielding, even low intensity events could present a non-trivial dose from low energy (<100 MeV) protons and should at least be considered before final mission architecture is defined.

Importantly, for a lightly shielded spacecraft, the dose from a large SEP event could substantially exceed that received from GCR radiation and therefore render the GCR contribution to the bio-response impossible to interpret. For example, based on the probabilistic estimates in Fig. 9 for 1 g/cm^2 Al shielding, an 18 mo mission would result in 50% chance that a dose of 15 cGy would be received from SEP events. This is compared with about 21 cGy during that time period from GCR alone. Added shielding would substantially reduce the dose contribution from SEP events, while not attenuating GCR significantly. Hence, differential shielding within the payload could be used as a strategy to obtain bio-response information for both GCR and SEP radiation.

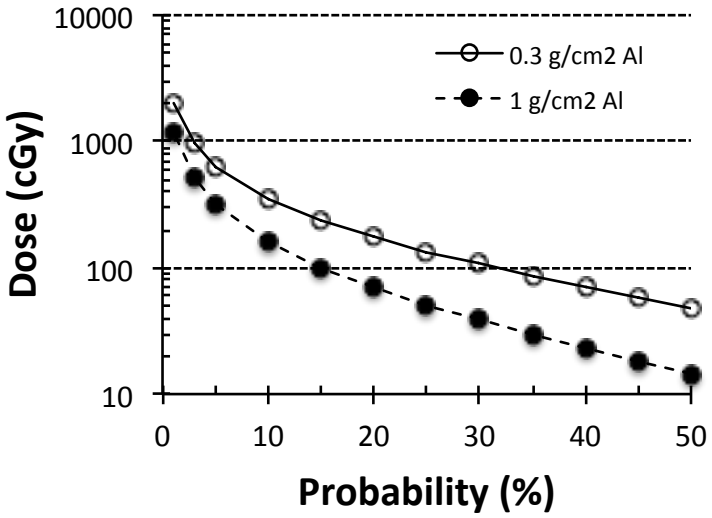

Figure 9. Probabilistic estimates of dose from SEP events in interplanetary space at 1 AU during solar maximum conditions. Based on Xapsos et al. 1999.

Conclusions

Space radiation modeling results are provided to help in the design of future biological experiments onboard missions beyond LEO. Nuclide-specific flux and dose rates were calculated using OLTARIS and these results were used to determine particle traversal rates and doses in selected biological targets. The lightest elements (H and He) have by far the highest flux and therefore traversal rates in biological targets, but heavy nuclides contribute substantially to the mean dose and dose equivalent for thin shielding and can produce large energy deposition in small biological targets such as cell nuclei. In interplanetary space, the total GCR spectrum would contribute less than 1 particle traversal per day to a cell nucleus, and less than one per year from the heaviest ions. Such rare (low dose rate) events must be considered in the design of biological experiments.

A comparison is provided between GCR in interplanetary space and inside the ISS. The radiation dose rate inside the ISS is below or approaching the lower limit of detection for most biological endpoints and has been a challenge for providing statistically significant radiobiological data when comparing with "unexposed" controls. Beyond LEO, the combination of higher dose rate and larger Q (i.e., relatively more high-LET particles)

increases the chances that biological effects may be detected, particularly for lightly shielded spacecrafts. This is a key justification for biosentinel-type experiments.

Large solar particle events could substantially impact biological experiments beyond LEO, especially for lightly shielded spacecraft. Large events are rare so they may not occur during a particular mission, but planning for them is prudent and could possibly be aided using payload shielding designs, i.e., SEPs are much easier to shield against than GCR.

Because of the many challenges associated with the success of such missions, extensive ground-based studies would be required to characterize a biological system prior to flight to determine that the response endpoints selected can be expected to be detected during the mission. This would include exposure to simulated space radiation available at accelerator facilities such as NSRL (La Tessa, et al. 2016). A major challenge would be the sensitivity of the biological system to the low-dose-rate GCR radiation environment in space, which is at or near the detection limit for most biological endpoints.

Acknowledgments

Work performed under the auspices of the NASA Ames Research Center, NASA Langley Research Center, and the Texas A&M University.

References

Akpa, T.C., Weber, K.J., Schneider, E., Kiefer, J., Frankenberg-Schwager, M., Harbich, R. and Frankenberg, D. (1992) Heavy ion-induced DNA double-strand breaks in yeast. Int. *J. Radiat. Biol.* 62:279-287.

Bhattacharya, S., Ricco, A.J, Hanel, R.P. and Crusan, J. (2016) http://www.nasa.gov/centers/ames/engineering/projects/biosentinel.html (accessed January 9, 2017).

Braby, L.A. (2008) A solution to the problem with absorbed dose. Nucl. Eng. Tech. 40:533-538.

Brooks, A., Bao, S., Rithidech, K., Couch, L.A. and Braby, L.A. (2001). "Relative effectiveness of HZE iron-56 particles for the induction of cytogenetic damage in vivo," Radiat. Res. **155**, 353–359.

Cucinotta, F.A., Kim, M.Y., Chappell, L.J., and Huff, J.L. (2013) How safe is safe enough? Radiation risk for a human mission to Mars. PloS ONE 8(10): e74988. doi:10.1371/journal.pone.0074988

Curtis, S.B. and Letaw, J.R. (1989) Galactic cosmic rays and cell-hit frequencies outside the magnetosphere. *Adv. Space Res.* 9:293-298.

Curtis, S.B. (2012) HZE fluence rates and energy depositions from delta rays: how important are they? 23 rd Annual NASA Space Radiation Investigator's Workshop, Durham, North Carolina, 2012.

Curtis, S.B. (2013) Fluence rates, delta rays and cell nucleus hit rates from Galactic cosmic rays.

George, K., Durante, M., Wu, H., Willingham, V., Badhwar, G. and Cucinotta, F.A. (2001) Chromosome aberrations in the blood lymphocytes of astronauts after space flight. *Radiat. Res.* 156:731–738.

George, K., Willingham, V. and Cucinotta, F.A. (2005) Stability of chromosome aberrations in the blood lymphocytes of astronauts measured after space flight by FISH chromosome painting. *Radiat. Res.* 164:474–480.

Hada, M. and Sutherland, B.M. (2006) Spectrum of complex DNA damages depends on the incident radiation. *Radiat. Res*. 165:223-230.

Haight, F.A. (1967) Handbook of the Poisson Distribution. New York: John Wiley & Sons.

Hathaway, D. (2016) http://solarscience.msfc.nasa.gov/predict.shtml (accessed August 18, 2016).

ICRP (2007). The 2007 recommendations of the International Commission on Radiological Protection, ICRP publication 103. Pergamon Press, Oxford.

Jorgensen, P., Edington, N.P., Schneider, B.L., Rupes, I., Tyers, M., and Futcher, B. (2007) The size of the nucleus increases as yeast cells grow. Molec. Biol. of the Cell 18:3523-3532.

Kiefer, J., Egenolf, R. and Ikpeme, S. (2002) Heavy ion-induced DNA double-strand breaks in yeast. *Radiat. Res.* 157:141-148.

La Tessa, C., Sivertz, M., Chang, I., Lowenstein, D., and Rusek, A. (2016) Overview of the NASA space radiation laboratory. *Life Science in Space Research.* 11: 18-23

Metting, N.F., Rossi, H.H., Braby, L.A., Kliauga, P.J., Howard, J., Zaider, M., Schimmerling, W., Wong, M. and Rapkin, M. (1988). "Microdosimetry near the trajectory of high-energy heavy ions," Radiat. Res. **116**, 183–195.

NASA (2016). https://www.nasa.gov/content/journey-to-mars-overview (accessed August 18, 2016).

NCRP (2006). Information needed to make radiation protection recommendations for space missions beyond low-earth orbit. NCRP report 153, Bethesda, MD.

Norbury, J.W. and Slaba, T. (2014) Space radiation accelerator experiments - the role of neutrons and light ions. *Life Sci. Space Res.* 3:90-94.

O'Neill, P.M. (2010) Badhwar-O'Neill galactic cosmic ray flux model – Revised. *IEEE Trans. Nuc. Sci.* 57:3148–3153.

Rostek, C., Turner, E.L., Robbins, M., Rightnar, S., Xiao, W., Obenaus, A., Harkness, T.A. (2008) Involvement of homologous recombination repair after proton-induced DNA damage. *Mutagenesis* 23:119-129.

Simpson, J. A. (1983) Elemental and isotopic composition of the galactic cosmic rays. *Ann. Rev. Nucl. Part. Sci.* 33:323-381.

Singleterry, R.C., Blattnig, S.R., Clowdsley, M.S., Qualls, G.D., Sandridge, C.A., Simonsen, L.C., Slaba, T.C., Walker, S.A., Badavi, F.F., Spangler, J.L., Aumann, A.R., Zapp, E.N., Rutledge, R.D., Lee, K.T., Norman, R.B. and Norbury, J.W. (2011) OLTARIS: On-line tool for the assessment of radiation in space. *Acta Astronautica* 68:1086-1097.

Straume, T. (2015) Medical Concerns with Space Radiation and Radiobiological Effects. In: Handbook of Cosmic Hazards and Planetary Defense (J. Pelton and F. Allahadi, Eds.), Springer International Publishing, Switzerland. This book chapter is also available for free download at the following URL: https://www.researchgate.net/profile/Tore_Straume (accessed August 18, 2018).

Todd, P. and J.T. Walker (1984) The Microlesion Concept in HZE Particle Dosimetry. *Adv. Space Res*. **4**:187-194.

Townsend, L.W. (2005) Implications of the space radiation environment for human exploration in deep space. *Radiat. Prot. Dosim.* 115:44-50.

Wilson, J.W., Cucinotta, F.A., Tai, H., Simonsen, L.C., Shinn, J.L., Thibeault, S.A. and Kim, M.Y. (1997) Galactic and solar cosmic ray shielding in deep space. NASA technical paper 3682. Available electronically at the following URL: http://techreports.larc.nasa.gov/ltrs/ltrs.html (accessed August 18, 2016).

Zeitlin, C., Hassler, D., Cucinotta, F., Ehresmann, B., et al. (2013) Measurement of energetic particle radiation in transit to Mars on the Mars Science Laboratory. *Science* 340:1080-1084.